Jurnal Teknologi Reaktor Nuklir

Tri Dasa Mega

Journal homepage: https://ejurnal.brin.go.id/tridam

Dose Optimization and Irradiation Angle Analysis for Advanced Liver Cancer Using PHITS Version 3.341

Ariana Irawati[1*], Beta Nur Pratiwi[1], Subur Pramono[1], Yohannes Sardjono[2], Isman Mulyadi Triatmoko[2], Gede Sutresna Wijaya[2], Heru Prasetio[2], Nur Rahmah Hidayati[2], Nunung Nuraeni[2], Syarifatul Ulya[2], Zuhdi Ismail[2]

[1] *Department of Physics, Faculty of Science, Sultan Maulana Hasanuddin State Islamic University, 42171, Banten, Indonesia*

[2] *Research Center for Safety, Metrology and Nuclear Quality Technology, Research Organization for Nuclear Energy, The National Research and Innovation Agency, Tangerang Selatan, Indonesia*

ARTICLE INFO

Article history:

Received: Dec 02, 2024
Received in revised form: Jan 13, 2025
Accepted: Jan 20, 2025

Keywords:

Liver Cancer
HCC
Fraction
Dosimetry
Radiotherapy
X-Ray Therapy
PHITS Version 3. 341

A B S T R A C T

Based on 2022 statistics from the World Health Organization (WHO), liver cancer ranks as the 3rd leading cause of cancer-related mortality worldwide, claiming approximately 750,000 lives annually. X-ray therapy has demonstrated effectiveness in providing local-regional control, making it a potential treatment modality for liver cancer. This study aims to determine the optimal irradiation direction for advanced-stage (C) Hepatocellular Carcinoma (HCC) using radiation therapy. To simulate the X-ray radiation transport process in the human body, a phantom model has been developed using various materials that mimic body tissues with the PHITS (Particle and Heavy Ion Transport code System) program Monte Carlo method. The study revealed that the irradiation direction greatly affects the irradiation time required to achieve the prescribed dose threshold. X-ray therapy dose analysis evaluates the number of fractions required to achieve a lethal dose to cancer cells while minimizing the dose to healthy surrounding cells. The irradiation direction was varied at 0°, 45°, and 90° to find the optimal angle that results in the shortest irradiation time. By evaluating the number of fractions needed to reach the lethal dose limit for cancer cells, the 45° or Right Anterior Oblique (RAO) irradiation direction is the most optimal direction with a total of 16-25 fractions with an irradiation time of 2.01 minutes/fraction and a dose to cancer of 1.94 Gy/fraction. These findings could contribute to the refinement of treatment protocols, which potentially improve outcomes for patients with advanced liver cancer.

© 2025 Tri Dasa Mega. All rights reserved.

1. INTRODUCTION

Based on statistical data from the WHO in 2022, liver cancer ranks 3rd out of 15 types of cancer that cause the global death toll to stand at 750 thousand, making it the leading cause of fatalities. The highest incidence of liver cancer cases is documented on the Asian continent, while in Indonesia, liver cancer ranks second as the highest cause of death. Available data shows that liver cancer cases are on the rise. The total number of new cases recorded in 2022 is around 860 thousand cases worldwide and 23 thousand cases in Indonesia [1]. This indicates a high mortality rate for liver cancer, reaching 87.60% globally and 98.23% in Indonesia, ranking it as the third and second highest cause of cancer-related deaths, respectively.

Current methods of liver cancer treatment include the use of drugs, surgical intervention, and

* Corresponding Author
Email: arianairawati20@gmail.com
DOI:10.55981/tdm.2025.7149

radiation therapy. However, the prognosis of using drugs tends to be unfavorable as the side effects of drug toxicity can cause damage to the liver and kidneys [2]. In addition, surgical interventions often pose a risk of postoperative complications and have a high recurrence rate [3]. Consequently, radiation therapy has become an important approach in managing liver cancer cases.

Radiotherapy is a medical approach that uses ionizing radiation to eliminate cancer cells within the patient's body, aiming to inflict maximum damage on cancer cells. At the cellular level, the most important impact of radiation is to damage DNA [4]. There are two types of cancer treatment using radiation, also known as radiotherapy, either internal or external. In internal radiation therapy, radioactive isotopes are inserted into the patient's body [5]. Meanwhile, in external radiation therapy, particles such as protons, neutrons, X-rays, or gamma rays are directed to the body [6]. The utilization of radiation for therapy and diagnostics is common, with the radiation source used being X-rays or photons.

Photons in radiotherapy can be generated using linear accelerators (LINAC) [7]. As of 2018, there are 49 LINACs spread throughout Indonesia [8]. A LINAC is a device that was originally designed to accelerate positively charged particles (protons) but was later modified to accelerate negatively charged particles (electrons), to near the speed of light [9]. The electrons accelerated by the LINAC can be used directly to treat tumors near the surface or focused on a specific target material to produce an X-ray beam, which is used to treat deeper tumor locations [7].

X-ray treatment is effective both as a single modality and combined to control tumors locally [10]. The medical application of X-rays in radiotherapy has been divided based on the energy produced by the radiation machine. High-energy machines (megavoltage, MV) are used in cancer therapy due to their ability to control radiation output with their collimator for skin protection and good tissue penetration. Conversely, low-energy devices (kilovoltage, kV) are primarily utilized in imaging techniques, including Computed Tomography (CT), mammography, and X-ray imaging of the chest or bones [10]. Based on the Minister of Health Regulation (PERMENKES) No. 24 of 2020, intermediate clinic radiology services are equipped with additional radiology equipment modalities such as bone densitometry, C-arm, and Magnetic Resonance Imaging (MRI) [11].

Magnetic Resonance Imaging (MRI) is a diagnostic technique that applies magnetic resonance within a magnetic field ranging from 0.064 to 1.5 Tesla (1 Tesla = 1000 Gauss) and utilizes the resonance of atomic nuclei to produce detailed images of the human body or its organs [12]. MRI produces high-resolution images and is more sensitive than X-rays or CT scans in assessing the soft tissue anatomy of the body [13]. MRI has the advantage of producing coronal, sagittal, axial, and oblique cross-sectional images without the need to change the patient's body position significantly. In addition, MRI makes it easier to identify organs at risk (OARs) around critical areas close to the target boundary [14]. As such, this technology is highly effective for detecting disruptions in soft tissue [12].

The Particle and Heavy Ion Transport code System (PHITS) is a nuclear radiation transport simulation software created by the Japan Atomic Energy Agency (JAEA) [15]. The PHITS program can model almost any type of radiation in three-dimensional (3D) geometry [16]. PHITS has the advantage of being able to simulate various particles with energies up to 1 TeV per nucleon [17], which is higher than other software, such as MCNPX, that limits the energy of X-rays to 100 GeV and electrons to 1 GeV. In addition, PHITS is designed for a wide range of applications, including radiation research, cancer therapy, and particle transport analysis, making it a more flexible and suitable choice for simulation needs. PHITS codes can calculate doses for different types of radiation. As such, PHITS can be used to simulate X-ray therapy beams using voxel or phantom models [18].

The importance of accurately selecting and applying ionizing radiation dosimetry, especially for low exposures, cannot be overstated. Dosimetry with high sensitivity is a crucial choice because it can accurately measure the amount of a patient's radiation exposure[19]. The use of proper radiation dose is important to consider before using X-ray radiation for tumor treatment. Higher doses can induce a higher potential for adverse effects, emphasizing the need for robust radiation protection protocols [20].

2. RESEARCH METHOD

Simulation of liver cancer therapy using X-ray therapy with the PHITS program aims to determine the optimal dose and direction of irradiation to maximize treatment effectiveness while minimizing damage to healthy tissue around the target area. The simulation process begins with the creation of a geometric model of the liver organ and surrounding tissues based on medical imaging data, such as CT or MRI. Next, the X-ray radiation source parameters, such as energy, intensity, and irradiation angle, were specified as an input for the PHITS program. Simulated data in the form of dose distribution for the target organ and surrounding tissues were analyzed to evaluate the

irradiation efficiency. The analysis involves the calculation of important parameters such as irradiation time, total absorbed dose, effective dose, and equivalent dose.

The reference phantom voxel selected was an adult American male Oak Ridge National Laboratory (ORNL) phantom, seen in **Figure 1.** The dimensions and configuration of the organ geometry are based on the ORNL phantom. However, in this simulation, the organs used are limited only to the middle part of the body, not the whole body. This simulation is more focused on the cancer cells found in the target organ, according to the type of case chosen.

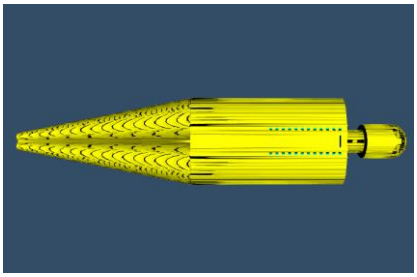

Figure 1. Phantom ORNL male American adult [21]

In addition, the system for X-ray therapy simulation was the ELEKTA Precise LINAC, specifically the Versa HD model [22]**.** Yaghmai et al's research in 2013 was used as one of the references to set parameters and project cancer cells in this study [23].

2.1. Modeling the shape of the patient's body and its organs

This study utilized the Monte Carlo method used in the PHITS program, which utilizes random probability to obtain precise results. In a medium, particles interact and move randomly. These relationships are stochastic but are influenced by the probability or response of the material to the particles. The process of movement and association between particles is referred to as particle transport. Particle transport calculations are crucial in the field of nuclear physics to understand various physical quantities associated with radiation [24].

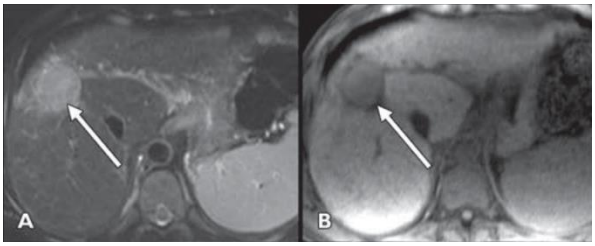

Figure 2. MRI imaging of a 56-year-old male patient with cirrhosis due to chronic hepatitis C virus infection and hepatocellular carcinoma (HCC). (A) A hyperintense HCC measuring 3.8 cm (marked by the arrow) is located in segment VIII. (B) The 3D unenhanced gradient-recalled echo (GRE) reveals that the HCC (indicated by the arrow) appears hyperintense [25].

To simulate the radiation transport process within the human body, phantoms have been created using a variety of materials that mimic human tissue. These phantoms are utilized to measure the radiation dose given to patients and to analyze the effectiveness of imaging systems [26]. A phantom was developed to replicate the imaging characteristics of body tissues. The specific phantom used is the ORNL model representing an adult American male [27]. This research focuses on individuals who have advanced primary liver cancer (C) with a tumor measuring 3.8 cm, as illustrated in Figure 2, where this stage of cancer is confined to the liver and has not metastasized to other areas of the body beyond the liver [28]. The total amount of radiation administered for this stage of liver cancer is approximately 30-50 Gy, with a daily dose ranging from 6 to 15 Gy, or around 45 to 50 Gy at a daily dose of 2 Gy [29].

The input file for each tumor volume was different for each organ, which will certainly affect the dose calculation for each phantom [30]. The heart geometry is defined as an elliptical cylinder truncated by a flat plane. Mathematically written as in (1)[27],

$$\left(\frac{x}{a}\right)^2 + \left(\frac{y}{b}\right)^2 \leq 1\,,$$
$$\frac{x}{x_m} + \frac{y}{y_m} - \frac{z}{z_m} \leq -1\,, \qquad (1)$$
$$z_2 \leq z \leq z_2$$

with the value of $a = 16.50$; $b = 8.00$; $x_m = 35.00$; $y_m = 45.00$; $z_m = 43.00$; $z_1 = 27.00$; $z_2 = 43.00\ cm$ and volume 1830 cm^3.

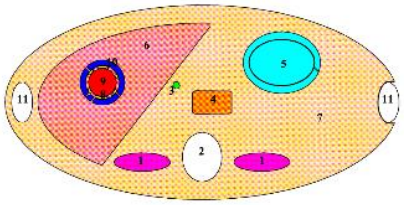

Description:
1. Kidney
2. Spine
3. Esophagus
4. Pancreas
5. Stomach
6. Liver
7. Soft tissue
8. CTV
9. GTV
10. PTV
11. Skeleton

Figure 3. Axial body tissue modeling in 2D

The Clinical Target Volume (CTV) is established by expanding the Gross Tumor Volume (GTV) margin by 2 to 4 mm. The Planning Target Volume (PTV) is defined by further expanding the CTV margin in three dimensions by 5 to 10 mm [31]. There is no standardized measurement for the CTV-PTV margin because of variations in body fixation methods and the accuracy of equipment

across different hospitals. This study utilized CTV with a margin of 2 mm and PTV with a margin of 5 mm, as illustrated in Figure 3. The cancer cell density in hepatocellular carcinoma (HCC) is 1.20 [32], while the density of the liver organ was 1.060 [33].

Organs at risk (OAR) of radiation exposure when treating liver cancer are the liver, heart, right kidney, esophagus, stomach, colon, and duodenum [34]. However, before the radiation hits these organs, it will pass through other tissues such as the skin and ribs.

2.2. Modeling a Linear Accelerator

The initial stage in this research is to create the geometry of the LINAC head with a tungsten target using the PHITS program. The X-ray mode of the LINAC head is made up of several components, including the target, primary collimator, flattening filter, monitor chamber, and secondary collimator (JAWS). For the simulation of X-ray calculations, the geometry includes a flattening filter, two pairs of block collimators, and a multi-leaf collimator. An incident beam with an energy of 10 MV and its corresponding energy distribution behind the metal target were used [19]. The simulation parameters are shown in Table 1**.**

Table 1. Parameters of the ray model in the simulation

No	Parameters	Description
1.	Beam energy [35]	10 MeV
2.	Particle [22]	Electron
3.	Beam intensity [22]	0.6653
4.	Normalization factor	1.12×10^{15}
5.	Size of beam	0.5 cm (radius)
6.	Irradiance angle variation [36]	$0°, 45°, 90°$
7.	SSD [37]	80 cm
8.	Particle count in the simulation	100.000
9.	Total batches in the simulation	50

When high-energy electrons collide with a heavy metal target, the LINAC produces high-energy X-rays used in radiotherapy procedures [7]. The accelerated electrons in a LINAC can also be directly utilized for radiotherapy without the need for heavy metals to generate X-rays. In this study, the target heavy metal used to generate X-rays was tungsten. The distance from the target area to the surface of the patient's skin is referred to as the Source Skin Distance (SSD). This distance is crucial in controlling the radiation dose administered to the patient. A greater SSD results in a reduced dose administered to the patient, usually a standard SSD size of 80 or 100 cm. However, in some situations, the SSD can be adjusted according to the patient's needs [37]. In this study, an SSD distance of 80 cm was used.

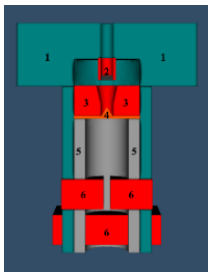

Description:
1. Outer shielding
2. Target (tungsten)
3. Primary collimator
4. Flattening filter
5. Shielding in
6. Secondary collimator (JAWS)

Figure 4. Linear Head Modeling of Accelerators

The angle of the irradiation beam is adjusted to align with the geometry of the organ's location that is to be simulated [30]. The irradiation was performed using the linear accelerator head design shown in Figure 4. The irradiation was performed with the beam from the front to the back of the phantom, or Anterior-Posterior (AP), with angles of 0°, 45°, and 90°, as shown in Figure 5.

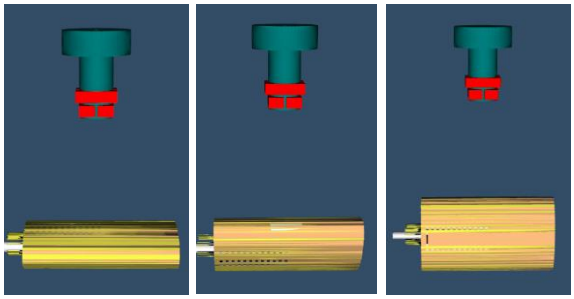

(a) (b) (c)

Figure 5. Visualization of the irradiation direction of X-ray therapy, (a) irradiation from the front to the back of the body (Anterior-Posterior (AP)), (b) irradiation from a 45° angle on the right front of the body (Right Anterior Oblique), (c) Irradiation from the right side of the body (Right Lateral) at a 90° angle on the right side.

The maximum energy generated by a 10 MV LINAC is 10 MeV. The X-ray energy generated by the 10 MV LINAC is 10 MeV. The requirement for this accelerator is that the vertical irradiation current beam at 10 MeV must be at least 1.8 mA [35]. The majority of electrons' kinetic energy converts to heat in the target, while a small fraction is released as X-rays, which are categorized into two groups: characteristic X-rays and bremsstrahlung X-rays. Operating tolerance of Linac model Versa HD $\pm$ 10%. Through the current, the normalization factor is obtained with (2) to determine the dose rate as follows [38],

$$Normalization\ factor = \frac{I\ [\mathrm{C/s}] \times T\ [\mathrm{s}] \times F}{charge\ per\ unit\ particle} \quad (2)$$

where I is the appliance current (A), T is the time (s), F is a Duty Factor (%), and the charge per unit particle used electron particle the charge is equal to $1{,}602 \times 10^{-19}\ C/s$. The normalization factor is used as a multiplier for the tally deposit parameter, resulting in the particle distribution.

2.3. Determine the Radiation Dose

Dose rate refers to the amount of radiation dose received per unit of time, where the dose represents either the amount of radiation in a radiation field or the quantity of radiation energy absorbed or encountered by a material. From the output dose rate obtained through simulation, irradiation time, equivalent dose, absorbed dose, and effective dose were calculated.

The irradiation time is calculated by dividing the minimum dose needed to damage cancer tissue by the dose rate, as shown in (4) [39]. In this context, the minimum dose that can damage cancerous tissue is 45 Gy.

$$irradiation\ time\ (s) = \frac{minimum\ dose\ of\ damage\ in\ cancer\ (Gy)}{total\ dose\ rate\ (Gy\ /\ s)} \quad (4)$$

Absorbed dose refers to the quantity of energy deposited in human tissue by radiation [26]. The use of the proper amount of radiation dose is important to consider before using X-ray radiation as a medical option. The higher the dose received, the greater the negative effects, so radiation protection is important [21].

Once the irradiation time is set, the dose received by the organ can be determined. The total dose is then analyzed to ensure it stays within the acceptable limits for healthy organs or Organs at Risk (OAR). The absorbed dose is calculated using equation (5)[40].

$$Absorbed\ dose\ (Gy) = Dose\ rate\ \left(\frac{Gy}{s}\right) \times iradiation\ time\ (s) \quad (5)$$

The standard unit for measuring absorbed dose is joules per kilogram (J/kg), and it is specifically referred to as Grays (Gy) [33]. The absorbed dose (Gy) is commonly used as the main metric for predicting therapeutic effects on tumors and potential side effects on normal tissues in both preclinical and clinical studies [41]. The maximum safe skin dose for radiation-induced reactions is 2 Gy. The tolerance threshold in the liver is 4.1 Gy per fractionation.

The equivalent dose (H_T) is calculated by multiplying the absorbed dose ($D_{T,R}$) by the radiation weighting factor (w_R), which indicates the relative effectiveness of different types of radiation in causing biological damage. Mathematically, the equivalent dose is obtained as (6) [33],

$$H_T = \sum_R w_R D_{T,R} \quad (6)$$

where H_T represents the equivalent dose, which assesses the effect of radiation on organ T, considering the type of radiation received. $D_{T,R}$ refers to the average absorbed dose received by an organ or tissue from radiation of a specific type R, and w_R is the radiation weighting factor. The w_R is applied to determine the equivalent dose based on the average absorbed dose to a tissue or organ. For instance, the weighting factor for X-ray radiation is w_R = 1 [33].

The effective dose (E) is the total of equivalent doses for all organs and tissues in a given body, weighted by the respective tissue factors, as expressed in (7) [33],

$$E = \sum_T w_T H_T \quad (7)$$

where E represents the effective dose, which quantifies the body's radiation risk. In this context, different organs' sensitivity to radiation is considered. H_T denotes the equivalent dose, and w_T Is the tissue weighting factor, a metric used to adjust the equivalent dose in an organ or tissue T to reflect its relative contribution to the total radiation-related stochastic effects [33]. In this study, the weight factors of skin and liver tissues were 0.01 and 0.04, respectively [42].

Percentage Depth Dose (PDD) refers to the percentage of the dose delivered at a specific depth relative to the dose at the maximum depth [43]. To determine the maximum dose and depth distribution that will be received by the patient's body, dose profile curves and percentage depth dose (PDD) are used [44].

3. RESULTS AND DISCUSSION

The absorbed dose in liver cancer therapy using X-ray therapy is obtained by processing the dose rate output from the therapy simulation with the PHITS program. The dose rate obtained is then compared with the minimum dose required to eliminate cancer cells, based on the referenced data. The output dose rate distribution from the PHITS simulation is illustrated in Fig. 6. and Fig. 7.

Figure 6 displays the radiation dose distribution in X-ray therapy for a liver cancer case. In Fig. 6(a), the dose distribution is shown for the anterior-posterior (AP) irradiation direction, in Fig. 6(b) for the Right Anterior Oblique (RAO) direction, and in Fig. 6(c) for the Right Lateral (RL) direction. In the AP direction, the body faces directly in front of the radiation source. In the RAO direction, the body is directed forward at an angle of 45 degrees to the

radiation source. Meanwhile, in the RL direction, the body faces to the left side, equivalent to an angle of 90 degrees from the front position. The colors in the figure reflect the radiation dose intensity, with red indicating the highest dose area focused on liver cancer cells as the target of therapy. Conversely, the blue color indicates lower radiation intensity, indicating minimal exposure to the surrounding healthy tissue. This distribution is designed to deliver optimal doses to the cancerous tissue in the liver while reducing radiation exposure to other organs and tissues outside the target area.

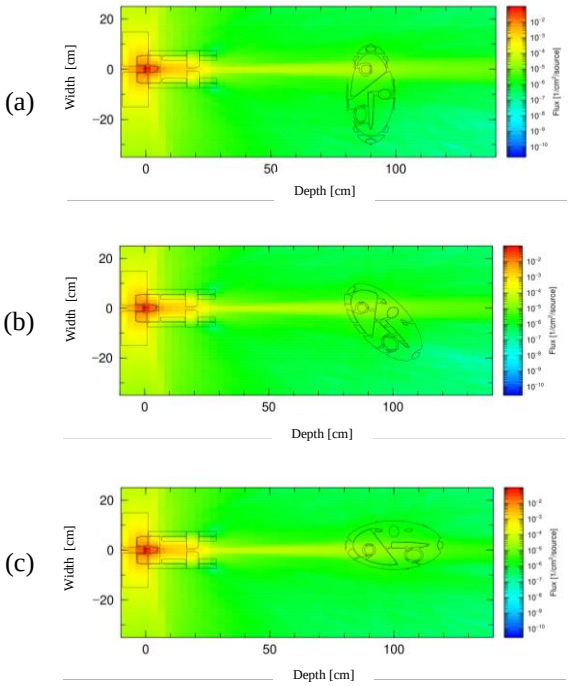

Figure 6. Simulated particle distribution, (a) Irradiation from front to back of the body (Anterior-Posterior (AP)), (d) Irradiation from 45° angle on the right front of the body (Right Anterior Oblique (RAO)), (c) Irradiation from the right side of the body (Right Lateral (RL)) 90° angle on the right.

Figure 7 displays the radiation dose distribution focused on the cancer cells with various irradiation directions. In Figure 7(a), the dose distribution is shown for the Anterior-Posterior (AP) irradiation direction, in Figure 7(b) for the Right Anterior Oblique (RAO) direction, and in Figure 7(c) for the Right Lateral (RL) direction. The horizontal axis indicates the depth of radiation penetration into the body, while the vertical axis represents the width of the exposure area. The colors in the figure depict the radiation dose intensity, where red indicates the area with the highest dose focused on the liver as the main target of therapy. In contrast, green to blue colors indicate areas of lower radiation intensity, reflecting decreased exposure to healthy tissue surrounding the target.

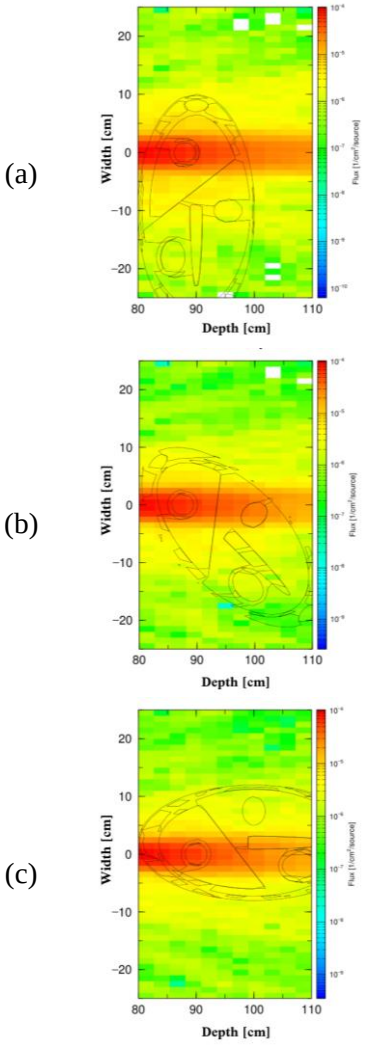

Figure 7. Particle distribution focused on liver cancer cells, (a) irradiation from front to back of the body (Anterior-Posterior (AP)), (b) irradiation at a 45° angle on the right front of the body (Right Anterior Oblique, (c) irradiation from the right side of the body (Right Lateral) at a 90° angle on the right).

The X-ray therapy dose rate graph shows how the radiation intensity varies at various depths in each tissue or medium. The difference in dose rate for different irradiation directions (0°, 45°, and 90°) is due to several main factors, including the size of the irradiation angle, the Compton effect, and photoelectricity. When X-rays enter the skin surface perpendicularly (at an angle of 0°), the radiation energy is spread more evenly throughout the tissue it passes through. Therefore, as shown in Figure 8, the dose rate will gradually decrease as the radiation energy is absorbed by the tissues along its path. At larger irradiation angles (e.g., 45° and 90°), the X-rays will take a longer path through the tissue before reaching the same point below the surface.

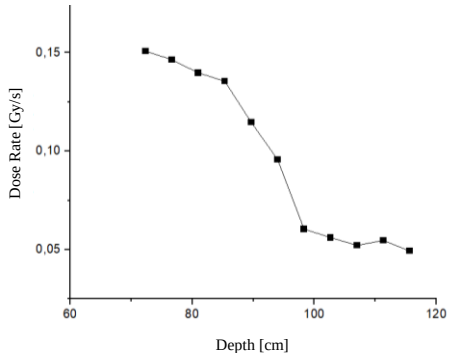

Figure 8. AP irradiation dose rate graph

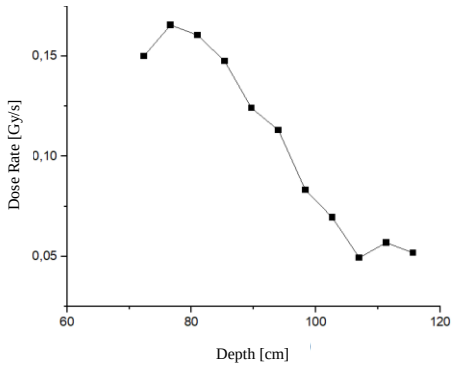

Figure 9. RAO irradiation dose rate graph

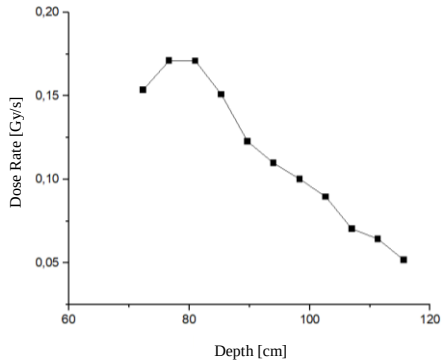

Figure 10. RL irradiation dose rate graph

This can increase the dose rate before reaching the skin because, at oblique angles, some of the X-ray energy may undergo reflection or Compton scattering, which amplifies the radiation dose in areas closer to the surface. Also, at larger angles, the longer path through the tissue can cause additional scattering, which increases the localized dose rate before reaching the skin surface. So, in the 45° and 90° angle dose rate graphs, there is an increase in the dose rate before reaching the skin, as seen in Fig. 9. and Figure 10.

From the three graphs, the dose rate data in the skin, liver, and cancer cells are obtained as shown in Table 2. After obtaining the dose rate for cancer cells (GTV), the irradiation time can be determined using calculations through equation (4). The radiation time needed so that the dose received does not exceed the dose threshold limit on body tissues, especially on the skin, which is 2 Gy. This is because the skin is the first tissue exposed to radiation directly. Irradiation time data is obtained in Table 3.

Table 2. Dose rate data simulated

Organ	Dose Rate (Gy/s)		
	AP	RAO	RL
Skin	0.014645	0.016559	0.017104
Liver	0.013975	0.016047	0.017097
GTV	0.013548	0.016047	0.015084
CTV	0.013548	0.016047	0.015084
PTV	0.013548	0.016047	0.015084

Table 3. Irradiation time and beam-on time

Angle of Irradiance	Total Treatment Time		Beam-on Time	
	seconds	minutes	seconds	minutes
AP	3562	59.4	137	2.28
RAO	3025	50.4	121	2.01
RL	3159	52.7	117	1.95

After obtaining the irradiation time and duration, the absorbed dose in one fraction is obtained through the calculation with equation (5), as shown in Table 4. The equivalent effective dose values can be calculated by multiplying the absorbed dose by the radiation weighting factors and the tissue weighting factors, as shown in Table 5.

Table 4. Absorbed dose in one fraction

Organ	Dose (Gy)			
	Dose Limit	AP (0°)	RAO (45°)	RL (90°)
Skin	2.0	2.00	2.00	2.00
Liver	4.2	1.91	1.94	2.00
GTV	2.0	1.85	1.94	1.76
CTV	2.0	1.85	1.94	1.76
PTV	2.0	1.85	1.94	1.76

Table 5. Simulated dose calculation

Angle of Irradiance	Number of fractions	Organ	Dose		
			Total absorption (Gy)	Equivalent (Gy)	Effective (Sv)
0°	26	Skin	52.2	52.2	0.52
		Liver	49.8	49.8	1.99
		GTV	48.3	48.3	-
		CTV	48.3	48.3	-
		PTV	48.3	48.3	-
45°	25	Skin	50.1	50.1	0.50
		Liver	48.5	48.5	1.94
		GTV	48.5	48.5	-
		CTV	48.5	48.5	-
		PTV	48.5	48.5	-
90°	27	Skin	54.0	54.0	0.54
		Liver	54.0	54.0	2.16
		GTV	47.7	47.7	-
		CTV	47.7	47.7	-
		PTV	47.7	47.7	-

Based on a review of the irradiation duration for one fraction in each direction, as shown in Tables 4 and 5, the Anterior-Posterior (AP) direction (front direction) requires a duration (Beam-on Time) of 2.28 minutes for each fraction, with a total fractions required to reach the dose limit capable of killing cancer cells of 26 fractions. In the 45° angle irradiation direction on the right front of the body (Right Anterior Oblique - RAO), the irradiation time of each fraction is 2.01 minutes, with a total of 25 fractions needed. Meanwhile, in the irradiation direction from the right side of the body (Right Lateral), the irradiation duration per fraction was 1.95 minutes, with a total of 27 fractions required. The dose per fraction and the total dose absorbed into cancer cells for irradiation angle of 0° are 1.85 Gy and 1.94 Gy, while at 45° are 1.76 Gy and 48.3 Gy, and at 90° are 48.5 Gy, 47.7 Gy.

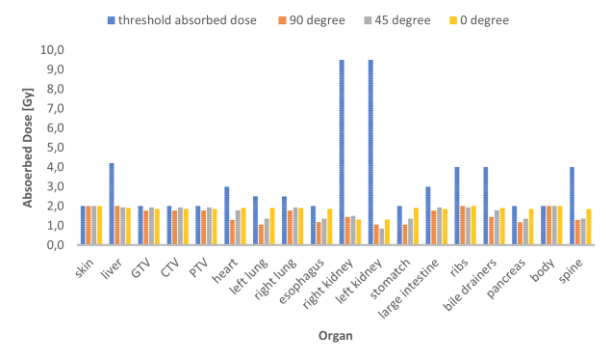

Figure 11. Absorbed dose of one-time fractionation

Figure 11 presents the absorbed dose data for each organ. The data show that the three variations of irradiation direction did not produce absorbed doses in one fraction that exceeded the safe absorbed dose tolerance threshold for the organ[45].

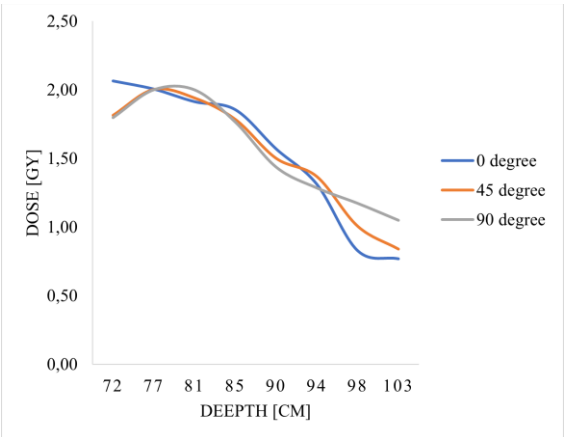

Figure 12. PDD graph of x-ray therapy simulation of three variations of irradiation direction (AP, RAO, RL)

The PDD graph shown in Figure 12 is in line with the PDD theory, which states that it will show a decrease in the context of X-ray therapy. This decrease in the PDD graph is influenced by several factors, including the Compton effect, photoelectric effect, and pair production effect. When X-rays are directed at an angle of 0 degrees, they are directed directly at the target tissue without any angle adjustment. At this angle, the X-rays only penetrate through a direct path to the tissue, which may lead to higher dose concentrations along the path. This increases the risk of uneven dose and excessive dose concentration in certain areas. In contrast, when X-rays are directed at a 45-degree angle, the angle creates optimal conditions for penetration into the tissue. At this angle, the X-rays spread more evenly, resulting in a more balanced dose distribution across the target area, especially in deeper tissues. At larger angles, such as at 90 degrees, the X-rays are directed perpendicular to the target surface, which results in a more complex dose distribution. At this angle, the X-rays pass through the tissue in multiple directions, creating a less controlled distribution pattern, and may reduce penetration efficiency in deeper tissues.

X-ray therapy relies on the interaction of X-rays and cells in the body, where hydrogen, as the main component of biological tissue, exhibits specific characteristics in radiation absorption. The main interaction of X-rays with body tissues occurs through the Compton effect, in which high-energy X-rays interact with electrons in hydrogen atoms. When an X-ray collides with an electron, some of the energy is transferred, causing the electron to accelerate and altering the X-ray's direction. This process results in scattering that reduces the energy of the remaining X-rays and contributes to a decrease in the radiation dose in the surrounding tissue. The photoelectric effect occurs when X-rays are absorbed by a material, decreasing the number of X-rays penetrating the tissue. Although the photoelectric effect is less common in hydrogen, it can also affect dose absorption in tissues, especially when X-rays have enough energy to be absorbed by electrons in the atom's shell. This effect leads to a loss of X-rays that can penetrate the tissue, reducing the dose that potentially damages healthy cells. Additionally, when high-energy X-rays interact with matter, they can produce electron-positron pairs. This pair production process reduces the X-rays' energy, further decreasing the number of X-rays able to penetrate the tissue.

At an angle of 45 degrees, most of the absorbed X-rays interact effectively with the tissue without exceeding the safe dose threshold. The PDD graph shows that the dose received by the tissue at a certain depth remains within safe limits, which is very important for preventing damage to healthy tissue. This shows that a 45-degree angle is not only

optimal for dose distribution, but also significantly reduces the risk of damage due to X-ray interaction with body tissues.

4. CONCLUSION

Based on the analysis of the beam-on time and the total number of fractions required for each irradiation direction, the 45° angle irradiation direction at the right front of the body (Right Anterior Oblique - RAO) is identified as the most optimal approach. RAO requires a relatively short irradiation time per fraction (2.01 minutes) and requires a smaller number of fractions (25 fractions) compared to other directions. Despite this efficiency, RAO still delivers an effective therapeutic dose capable of killing cancer cells. Up to 1.94 Gy per fraction, with a total absorbed dose of 48.5 Gy. This finding demonstrates that RAO is an efficient choice in terms of time management and the number of fractions required to achieve an effective therapeutic dose in killing cancer cells.

ACKNOWLEDGMENT

This research could not have been realized without the support, direction, and valuable contributions from various parties. Therefore, with all due respect, we would like to express our gratitude to:

1. The Ministry of Education, Culture, Research, and Technology (KEMENDIKBUD), as well as the Research Center for Nuclear Safety, Metrology, and Quality Technology of the National Research and Innovation Agency (BRIN), has established the MBKM (*Merdeka Belajar Kampus Merdeka*) internship program.
2. The Ministry of Religious Affairs (KEMENAG) plays an important role in the cooperation of this MBKM program.
3. UIN Sultan Maulana Hasanuddin Banten, who has provided knowledge, criticism, and suggestions during the completion of this research.
4. Japan Atomic Energy Agency (JAEA) for providing the PHITS program, which is very helpful for this research.

AUTHOR CONTRIBUTION

Ariana Irawati: Ideas, formulation or evolution of overarching research goals and aims, development or design of methodology, creation of models, programming, software development, designing computer programs, implementation of the computer PHITS code and supporting algorithms, testing of existing PHITS code components; **Beta Nur Pratiwi:** Verification, whether as a part of the activity or separate, of the overall replication/ reproducibility of results/experiments and other research outputs; **Subur Pramono:** Application of statistical, mathematical, computational, or other formal techniques to analyze or synthesize study data; **Yohannes Sardjono:** Conducting a research and investigation process, specifically performing the experiments, or data/evidence collection; **Gede Sutresna Wijaya:** Provision of study materials, reagents, materials, patients, laboratory samples, animals, instrumentation, computing resources, or other analysis tools; **Isman Mulyadi Triatmoko:** Management activities to annotate (produce metadata), scrub data and maintain research data (including software PHITS code, where it is necessary for interpreting the data itself) for initial use and later reuse; **Nunung Nuraeni:** Preparation, creation and/or presentation of the published work, specifically writing the initial draft (including substantive translation); **Heru Prasetio:** Preparation, creation and/or presentation of the published work by those from the original research group, specifically critical review, commentary or revision – including pre-or postpublication stages; **Nur Rahmah Hidayati:** Preparation, creation and/or presentation of the published work, specifically visualization/ data presentation; **Syarifatul Ulya:** Oversight and leadership responsibility for the research activity planning and execution, including mentorship external to the core team cancer therapy; **Zuhdi Ismail:** Management and coordination responsibility for the research activity planning and execution.

REFERENCES

1. Ferlay J., Ervik M., Lam F L.M.C.M., Mery L., Piñeros M., Znaor A., et al. Global Cancer Observatory: Cancer Today. 2022 ed. Lyon, France: International Agency for Research on Cancer; 2024.
2. Song X., Hou K., Zhou H., Yang J., Cao T., Zhang J. *Liver Organoids and their Application in Liver Cancer Research*. Regenerative Therapy.Japanese Society of Regenerative Medicine; 2024.
3. Orcutt S.T., Anaya D.A. *Liver Resection and Surgical Strategies for Management of Primary Liver Cancer*. Cancer Control.SAGE Publications Ltd; 2018.
4. Vaidya J.S. Principles of Cancer Treatment by Radiotherapy. Elsevier. 2024. 42(3):139–49.
5. Vilgrain V., Pereira H., Assenat E., Guiu B., Ilonca A.D., Pageaux G.P., et al. Efficacy and Safety of Selective Internal Radiotherapy with Yttrium-90 Resin Microspheres Compared with

Sorafenib in Locally Advanced and Inoperable Hepatocellular Carcinoma (SARAH): an Open-label Randomised Controlled Phase 3 trial. Lancet Oncol. 2017. 18(12):1624–36.
6. Smith S., Prewett S. *Principles of Chemotherapy and Radiotherapy*. Obstetrics, Gynaecology and Reproductive Medicine.Churchill Livingstone; 2017.
7. Nurmansya V.A., Winarno, Miskiyah Z. Radioterapi Kanker Cervix dengan Linear Accelerator (LINAC). J. Biosains Pascasarj. 2021. 23(02)
8. PORI *Program Kerja Perhimpunan Dokter Spesialis Onkologi Radiasi Indonesia*. 2018.
9. Fitriatuzzakiyyah N., Sinuraya R.K., Puspitasari I.M. Cancer Therapy with Radiation: The Basic Concept of Radiotherapy and Its Development in Indonesia. Indones. J. Clin. Pharm. 2017. 6(4):311–20.
10. Breitkreutz D.Y., Weil M.D., Bazalova-Carter M. *External Beam Radiation Therapy with Kilovoltage X-rays*. Physica Medica.Associazione Italiana di Fisica Medica; 2020.
11. Peraturan Menteri Kesehatan *Pelayanan Radiologi Klinik*. 2020.
12. Prita, Prasetya I.M.L., Restiana Prosedur Pemeriksaan Magnetic Resonance Imaging (MRI) Pelvis Menggunakan Kontras Pada Kasus Fistula. J. Ilmu Kedokt. dan Kesehat. 2023. 10(10)
13. Jatmiko A.W., Chendra Arum Wandani, Linda Wahyu Istigfarisky Efek Pemakaian Kontras Untuk Optimalisasi Citra Pada Pemeriksaan Diagnostik Magnetic Resonance Imaging (MRI). J. Biosains Pascasarj. 2021. 23(1):28.
14. Elguindi S., Zelefsky M.J., Jiang J., Veeraraghavan H., Deasy J.O., Hunt M.A., et al. Deep Learning-based Auto-segmentation of Targets and Organs-at-risk for Magnetic Resonance Imaging only Planning of Prostate Radiotherapy. Phys. Imaging Radiat. Oncol. 2019. 12:80–6.
15. Sardjono Y., Walhikmah R., Widiatmono R., Mahmudah R.S.N., Wijaya G.S., Triatmoko I.M., et al. Safety Analysis of Paraffin Wax-based Biological Shielding for Cancer Therapy with BNCT Method on Piercing Beamport of Kartini Nuclear Reactor, Yogyakarta. in: *Journal of Physics: Conference Series*. 2022.
16. Abdul Aziz M.Z., Yani S., Haryanto F., Ya Ali N.K., Tajudin S.M., Iwase H., et al. Monte Carlo Simulation of X-ray Room Shielding in Diagnostic Radiology using PHITS Code. J. Radiat. Res. Appl. Sci. 2020. 13(1):704–13.
17. Sato T., Iwamoto Y., Hashimoto S., Ogawa T., Furuta T., Abe S.I., et al. Recent Improvements of the Particle and Heavy Ion Transport Code System–PHITS version 3.33. J. Nucl. Sci. Technol. 2024. 61(1):127–35.
18. Takada K., Kumada H., Matsumura A., Sakurai H., Sakae T. Computational evaluation of dose distribution for BNCT treatment combined with X-ray therapy or proton beam therapy. Appl. Radiat. Isot. 2020. 165
19. Fuadi N., Jusli N., Harmini Pemantauan Dosis Perorangan Menggunakan Thermoluminescence Dosimeter (TLD) di Wilayah Papua dan Papua Barat Tahun 2020-2021. 2022. 2(1):63–74.
20. Aryawijayanti R., Susilo S. Analisis Dampak Radiasi Sinar-X pada Mencit Melalui Pemetaan Dosis Radiasi di Laboratorium Fisika Medik. J. MIPA. 2015. 38(1):25–30.
21. Elekta AB *Elekta Versa HD ™*. 2019.
22. Sardjono Y., Harto A.W., Arrozi M.I.M., Irhas, Santoso B.H., Tanthawi H. Pengantar Monte Carlo N-Particle Dasar-dasar perancangan fasilitas Boron Neutron-capture Cancer Therapy. Yogyakarta:Jogja Bangkit Publisher; 2015..
23. Jamal N.H.M., Sayed I.S., Syed W.S. Estimation of Organ Absorbed Dose in Pediatric chest X-ray Examination: A Phantom Study. Radiat. Phys. Chem. 2020. 166
24. Krstić D., Marković V., Živković M. Primena Monte Carlo Progama I Fantoma U Dozimetriji. Kragujevac:Fakultas Sains, Universitas Kragujevac Radoja Domanovića; 2023.
25. Schütte K., Schinner R., Fabritius M.P., Möller M., Kuhl C., Iezzi R., et al. Impact of Extrahepatic Metastases on Overall Survival in Patients with Advanced Liver-Dominant Hepatocellular Carcinoma: A Subanalysis of the SORAMIC Trial. Liver Cancer. 2020. 9(6):771–86.
26. Fukumitsu N., Okumura T., Sakurai H. *Radiotherapy for Liver Cancer*. Journal of General and Family Medicine.Wiley-Blackwell; 2017.
27. Setiawati E., Susanto R.E., Arianto F. Penentuan Faktor Koreksi Dosis Radiasi Sinar-X Linac 6 MV Pada Ketidakhomogenan Jaringan Tubuh dengan MCNPX. J. Ilm. Apl. Isot. dan Radiasi. 2022. 18(1):17.
28. Ito F., Kawai Y., Nakamura M., Toyama H., Hayashi S. Liver function and Image Evaluation after radiotherapy for liver metastases after resection of sigmoid colon cancer: a case report. Int. J. Surg. Case Rep. 2024. 116
29. Yan M., Yao J., Lin Y., Yan J., Xie Y., Fu Z.,

et al. Tumor Cell Density-dependent IL-8 secretion induces the fluctuation of tregs/CD8 + T Cells Infiltration in Hepatocellular Carcinoma: one Prompt for the Existence of a Density Checkpoint. J. Transl. Med. 2023. 21(1)

30. ICRP Adult Mesh-type Reference Computational Phantoms Annals of the ICRP Publication 145. ICRP Publ. 145. 2020. 49(3)
31. Schmid R.K., Tai A., Klawikowski S., Straza M., Ramahi K., Li X.A., et al. The Dosimetric Impact of Interfractional Organ-at-Risk Movement During Liver Stereotactic Body Radiation Therapy. Pract. Radiat. Oncol. 2019. 9(6):e549–58.
32. Zhang S., Zhang Z.D., Iqbal M., Chi Y.L. Physical Design of A 10 MeV Electron Linac For Industrial Application and Material Irradiation Effect Research. 2022.
33. Pratama M.A.A. *Penatalaksanaan Terapi Radiasi Eksterna Teknik 3D-CRT pada Kasus Kanker Serviks di Instalasi Radioterapi RSUD Arifin Achmad Provinsi Riau*. Pekanbaru:Sekolah Tinggi Ilmu Kesehatan Awal Bros; 2021.
34. Nurhadi I.D., Ramdani R., Haryanto F., Perkasa Y.S., Sanjaya M. Analisis Pengaruh Perubahan Source to Surface Distance (SSD) dan Field Size terhadap Distribusi Dosis menggunakan Metode Monte Carlo-EGSnrc. Pros. SNIPS. 2016.
35. Ihya F.N., Anam C., Gunawan V. Pembuatan Kurva Isodosis 2D Dengan Menggunakan Kurva Percentage Depth Dose (Pdd) dan Profil Dosis dengan Variasi Kedalaman Untuk Treatment Planning System. Berk. Fis. 2013. 16(4):131–8.
36. Sato T., Iwamoto Y., Hashimoto S., Ogawa T., Furuta T., Abe S., et al. User's Manual PHITS Ver. 3.34. in: *User's Manual PHITS*. English Version ed. 2024.
37. Harish A.F., Warsono, Sardjono Y. Dose Analysis of Boron Neutron Capture Therapy (BNCT) Treatment for Lung Cancer Based on Particle and Heavy Ion Transport Code System (PHITS). ASEAN J. Sci. Technol. Dev. 2020. 35(3):187–94.
38. Sato T., Furuta T., Liu Y., Naka S., Nagamori S., Kanai Y., et al. Individual Dosimetry System for Targeted Alpha Therapy based on PHITS Coupled with Microdosimetric Kinetic Model. EJNMMI Phys. 2021. 8(1)
39. Emami B. Tolerance of Normal Tissue to Therapeutic Radiation. Dep. Radiat. Oncol. 2013. 1(1):41.
40. BATAN Proteksi dan Keselamatan Radiasi Batan. Standar Batan Bid. Adm. Manaj. dan Organ. 2014.
41. Jusmawang, Syamsir Dewang, Bidayatul Armynah *Analyzes The Characteristics Of Percentage Depth Dose (Pdd) And The Profile Dose Device Linear Accelerator (Linac) For The X-Ray Beam With Variation Area Of Irradiation Field*. Makassar: 2015.
42. Mariatul Khiftiyah, Eko Hidayanto, Zaenal Arifin Analisa Kurva Percentage Depth Dose (PDD) dan ProfileDose untuk Lapangan Radiasi Simetri dan Asimetri PadaLinear Accelerator (LINAC) 6 dan 10 MV. Youngster Phys. J. 2014. 3(4):279–86.
43. Cefaro G.A., Genovesi D., Perez C.A., Valentini V. Delineating Organs at Risk in Radiation Therapy.Springer-Verlag Italia s.r.l.; 2013.
44. Gerhard S.G., Palma D.A., Arifin A.J., Louie A. V., Li G.J., Al-Shafa F., et al. *Organ at Risk Dose Constraints in SABR: A Systematic Review of Active Clinical Trials*. Practical Radiation Oncology.Elsevier Inc.; 2021.
45. Chang D.S., Lasley F.D., Das I.J., Mendonca M.S., Dynlacht J.R. Normal Tissue Radiation Responses. in: *Basic Radiotherapy Physics and Biology*.Springer International Publishing; 2014. pp. 265–75.